ChemEurJ

Research Article
doi.org/10.1002/chem.202502440

Chemistry Europe
European Chemical Societies Publishing

www.chemeurj.org

Selective Recognition of Physiological Phosphates by Luminescent Europium(III) Probes via Analyte-Specific Energy-Transfer Pathways

Goutam Panigrahi,[a] Sunanda Pradhan,[a] Nitin Shukla,[a] and Ashis K. Patra*[a]

The physiological phosphates (PPs) are crucial in various biochemical pathways and bioenergetics. Their dysregulation is associated with multiple cellular dysfunctions and life-threatening diseases. Designing sensitive and selective bioresponsive probes capable of differentiating Pi/NPPs levels is crucial for diagnostics and therapy. Developing probes for selective discrimination of phosphates faces intrinsic challenges due to their high hydration energy (ΔG_{hyd}) barrier and structural similarity. The hard Ln(III) ions can overcome the high ΔG_{hyd} barrier and are ideal for the detection and discrimination of PPs due to their longer lifetimes, using time-resolved luminescence (TRL) assays. Herein, two water-soluble luminescent Eu(III) probes, [**Eu.L1**] and [**Eu.L2**], can discriminate physiological inorganic (Pi) and nucleoside polyphosphates (NPPs) in H_2O based on their differential binding interaction with the respective probe, triggering analyte-specific energy-transfer pathways. We established the involvement of coordinative unsaturation and π-π stacking interaction between the [**Eu.L**] probes and PPs, which modulates the nonradiative vibrational energy transfer (VET) and photo-induced electron transfer (PeT) pathways, responsible for their specific luminescence response and selectivity. The interaction of phosphates with the Eu(III) probes were monitored by TRL spectroscopy, lifetime (τ) and hydration state (q) measurements, and ^{31}P NMR spectroscopy. These results connect the intricate molecular interactions of the [**Eu.L**] probes with PPs with concomitant TRL-responses.

1. Introduction

The physiological phosphates (PPs), comprising both inorganic and organic phosphates, play a variety of essential functions and regulate critical biochemical pathways in living organisms.[1–3] Inorganic phosphates (e.g., HPO_4^{2-} (Pi); $P_2O_7^{4-}$ (PPi)) play key roles in the synthesis of ATP and as components of hard skeletal tissues. The NPPs and their derivatives play crucial roles in bioenergetics, metabolism, protein phosphorylation, and associated signal transduction or cellular signaling, precursors of nucleic acid (DNA/RNA) biosynthesis.[2–5] NPPs are also key in essential enzymatic reactions, including GTPases, kinases, glycosyltransferases (GTs), etc. Any dysregulation from the normal homeostatic level of these Pi (physiological inorganic phosphates) and NPPs is directly associated with hyperphosphatemia, hypoparathyroidism, metabolic and respiratory acidolysis, chronic kidney diseases, neurodegenerative diseases, cancer, etc.[6–10] Hence, developing sensitive and selective bioresponsive probes capable of differentiating Pi or NPPs levels or their ratios is important for high-throughput screening (HTS) of enzyme inhibitors for drug discovery and disease diagnostics.[11,12] Distinguishing between these Pi/NPPs in a biological solvent medium is challenging and truly complex due to their structural similarity, limited recognition sites, pH-sensitive ionic charges, and necessity for overcoming high hydration energy (ΔG_{hyd}) barriers and low concentration of PPs compared to other common competing anions (e.g., Cl^-, lactate, HCO_3^-) in intracellular fluid.[13,14] Organic probes with poor solubility and stability in water and that lack desirable selectivity or sensitivity to PPs due to weak intermolecular interactions with hard phosphates that are unable to overcome high ΔG_{hyd}.[3] Unlike organic chemosensors, hard Ln(III) ions electrostatically interact with hard phosphates that overcome their high ΔG_{hyd} barrier in water.[3] Several design approaches derived from these molecular interactions have been used recently to create molecular optical probes that selectively bind to NPPs.[15–19] The antenna-sensitized Ln(III) probes with unique optical features offer sharp $f \rightarrow f$ emission bands in the vis-NIR range, sensitive to perturbation of EnT-pathways and changes in local chemical environment around Ln(III) upon interaction with PPs and serve as a reliable optical yardstick for real-time monitoring of Pi/NPPs in biological media.[20–22] Importantly, the longer excited state lifetimes (μs-ms) enable time-resolved luminescence (TRL) measurements, eliminating short-lived autofluorescence, yielding high S/N and sensitivity, highly desirable for biological assays.[20–34] The selectivity for the specific PPs could be fine-tuned by providing complementary open binding pockets and noncovalent interaction sites (e.g., hydrophobic stacking, H-bonding, etc.) based on the structure, charge, and steric constraints.[24] The exploitation of

[a] G. Panigrahi, S. Pradhan, N. Shukla, Prof. A. K. Patra
Department of Chemistry, Indian Institute of Technology Kanpur, Kanpur, Uttar Pradesh 208016, India
E-mail: akpatra@iitk.ac.in

Supporting information for this article is available on the WWW under https://doi.org/10.1002/chem.202502440

analyte-specific certain ET-mechanism(s) from the antenna/deactivation mechanisms or their combination triggered by their differential molecular interaction(s) with the emissive Ln(III) probe is an important strategy to achieve discrimination between structurally analogous Pi or NPPs.[35] A cautious design of a chelating antenna can tune the open coordination site(s) at the Ln(III) ion with bound H_2O (q), resulting in luminescence quenching by vibrational energy transfer (VET) from Ln(III)* to O-H oscillator. The binding of hard anionic PPs replaces H_2O and relieves the nonradiative VET quenching, thus increasing the lifetime (τ) and luminescence intensity.[36–40] The probe can also provide additional selectivity for challenging NPPs by perturbing the ET-mechanism (e.g., PeT) via noncovalent interaction (e.g., H-bonding, π-π interaction, etc.) with the antenna.[36] Luminescent Ln(III)-based probes for the selective identification of different NPP anions and their use in tracking various enzyme activities (e.g., kinase activity) have recently emerged as a niche research area in drug discovery assays.[41–44] Albrecht and coworkers developed coordinatively unsaturated Eu(III)-helicates for selective luminescence enhancement response for AMP in the presence of ADP and ATP due to favorable complementary receptor–analyte interactions. Here, the two Eu(III) centers were thought to be bridged due to perfect shape and size match of AMP, which displaces the labile solvent or counteranions and produces selectivity and increased luminescence intensity with AMP.[45] Pierre *et al*. performed an in-depth evaluation for a series of water-soluble coordinatively unsaturated macrocyclic Eu(III)-HOPO (hydroxy pyridonate)-derived complexes and studied the combination of various factors (i.e., C.N., q value, H-bonding, electrostatic interactions, etc.) that may potentially facilitate selective binding with Pi in the presence of other common oxyanions.[46] Butler *et al*. developed a novel Eu(III) probe, [Eu.ADPGlow]$^-$, containing a phenoxy acetate-functionalized quinoline antenna-based cyclen scaffold. This probe can monitor dynamic ADP levels in the presence of AMP and ATP, making it a viable tool for real-time cellular ADP visualization.[47] Recently, we reported a series of water-soluble luminescent Tb(III) probes with aromatic amino acids on the DTTA chelator: [Tb-L^{aa}], that preferentially discriminate guanine-NPPs over adenine-NPPs via PeT-based quenching of Tb(III) luminescence.[48]

Herein, we report two water-soluble thermodynamically stable cationic luminescent Eu(III) probes, *viz*. [**Eu.L1**] and [**Eu.L2**], containing pyridine-diaza-15-crown-5 macrocyclic chelates (**H_2L**) containing two anionic carboxylate pendant arms, allowing strong ionic bonding between CO_2^- and Eu(III). Subtle rational structural changes in **H_2L1/L2** were achieved by introducing 6-methyl-pyridine-2-carboxylate, which resulted in the variation of C.N., steric constraint, and capability for π-π stacking interaction with planar nucleobases. These changes are envisioned to significantly modulate the mode of binding, binding affinity, and trigger Pi/NPPs-specific ET-mechanism(s) for sensitization of Eu(III) for TRL-based selective sensing by **[Eu.L1]** and [**Eu.L2**] (Figure 1).

2. Results and Discussion

2.1. Molecular Design

Two macrocyclic cationic Eu(III) probes were synthesized that provide steric constraints and rigidity around the Eu(III) centers to allow mono-/ bi-dentate binding of phosphates while avoiding the chelation of common oxyanions.

The aromatic pyridine ring in the macrocyclic moiety acts as an efficient sensitizer to Eu(III) for $^5D_0 \rightarrow {}^7F_J$ transitions in the visible red region. The two anionic acetate pendant arms are meticulously placed to facilitate a favorable strong ionic interaction between Eu^{3+} and CO_2^-, which prevents leaching out of Eu(III) in biological media and provides thermodynamic and kinetic stability of the probe. The mono-cationic [**Eu.L**] probes are capable of a strong electrostatic interaction with anionic phosphate ions at physiological pH. Systematically tuning the pendant arms from acetate in **H_2L1** to 6-methyl-pyridine-2-carboxylate in **H_2L2** increased the coordination number (C.N.) of Eu(III) from 7 ($q = 2$) in [**Eu.L1**] to 9 ($q = 0$) in coordinatively-saturated [**Eu.L2**] with surrounding steric constraint around Eu(III) centre. The planar pyridine ring could potentially provide additional selectivity via noncovalent π-π stacking interaction with the planar adenine/guanine base of nucleoside polyphosphates (NPPs) (Figure 1).

2.2. Synthesis and Characterization

The pyridine-diaza-15-crown-5-based macrocyclic chelates (**H_2L1** and **H_2L2**) were synthesized using multistep syntheses (Figure 2).

The coordinatively unsaturated [**Eu.L1**] probe was synthesized from the previosly reported **H_2L1** macrocyclic chelate with seven coordination sites,[49] and used for selective discrimination of Pi/PPi and among mono-, di-, and tri-nucleoside phosphates. To gain better insights on the molecular interactions between [**Eu.L1**] and various PPs, 6-methyl-pyridine-2-carboxylate moiety was introduced in **H_2L2** providing with nine binding sites for coordinatively-saturated [**Eu.L2**] probe, offering differential binding interaction(s) by the ligand environment. In the above synthetic scheme, intermediates **1**–**3** were synthesized following the literature procedures.[50–54] The unreported intermediate **4** was synthesized by following a modified literature method.[55] In brief, the -NH_2 group of 1,8-diamino-3,6-dioxaoctane was protected by treating with 2-nitrophenylsulfonyl chloride (*o*-NsCl) in DCM using Et_3N at RT to yield **4**. The cyclization with 2,6–bis(bromomethyl)pyridine (**3a**) in the presence of K_2CO_3 under reflux in dry MeCN afforded **5**. The deprotection of nitrosyl group in **5** using thiophenol gave the corresponding free macrocycle **6**. The compound **6** upon reaction with 2 equiv. of methyl bromoacetate (for **H_2L1**)/ methyl 6-(bromomethyl) picolinate (for **H_2L2**) in dry MeCN in the presence of K_2CO_3 under reflux afforded carboxylate-protected **7a** and **7b**, respectively. The ester hydrolysis of **7a/7b** using 6 M HCl afforded the corresponding polyamino-carboxylate ligands **H_2L1/L2**. The complexation with

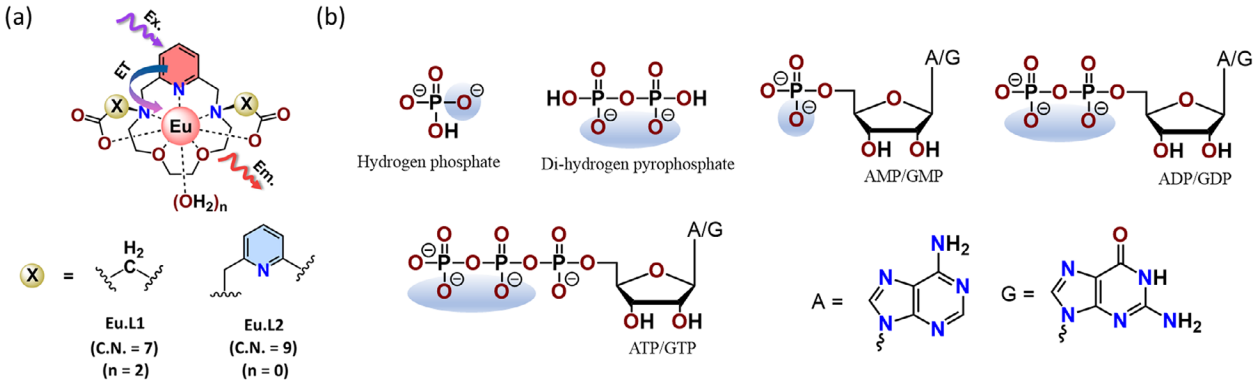

Figure 1. a) Proposed structure of Eu(III) probes ([**Eu.L1**] and [**Eu.L2**]) showcasing the ET-pathways. **b)** The chemical structures and highlighted phosphate-binding moieties of the inorganic (Pi, PPi) and organic physiological phosphates (PPs) used in this study.

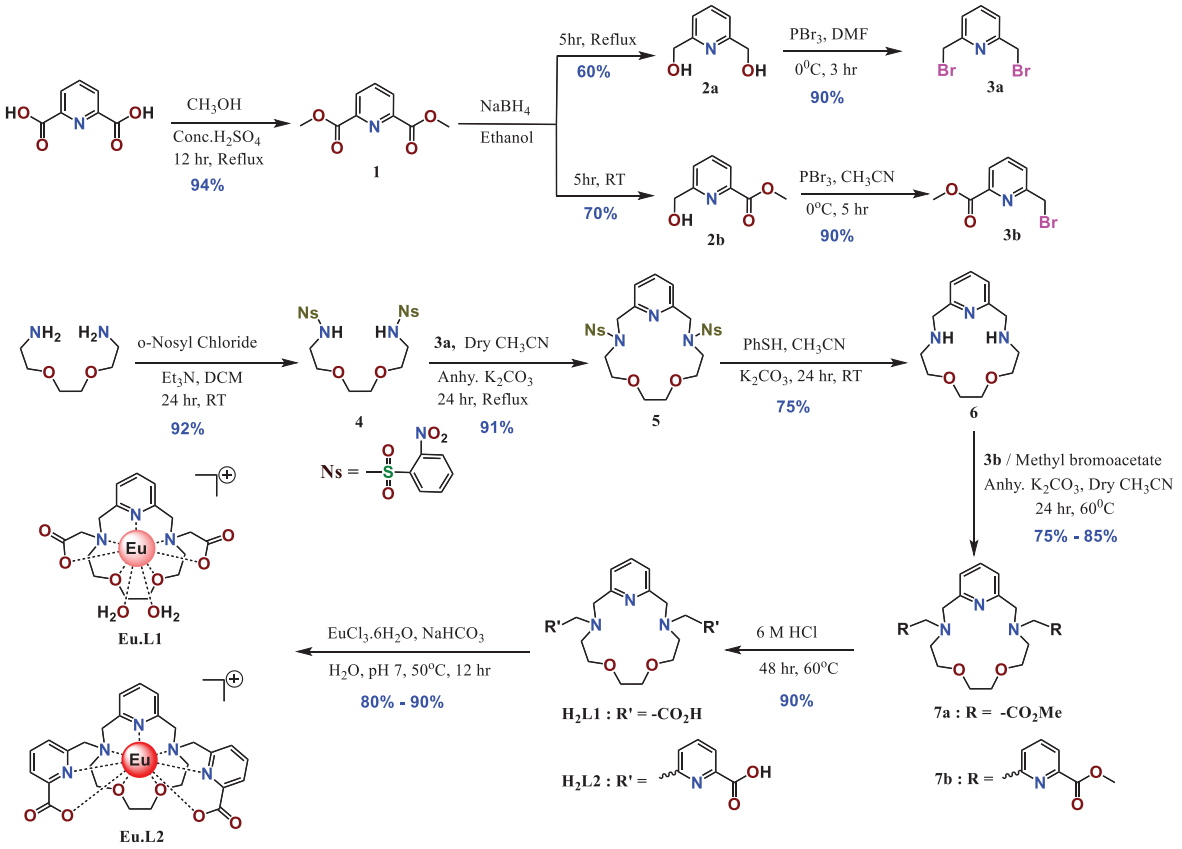

Figure 2. Synthetic scheme for the preparation of ligands (H_2**L1** and H_2**L2**) and Eu(III) complexes (**Eu.L1**, **Eu.L2**).

Eu(III) was carried out by reacting 1 equiv. of Eu(III) salts and 1 equiv. of H_2**L1**/H_2**L2** at pH 7 in water at 50 °C for 12 hours. The ligands were thoroughly characterized using $^{1}H/^{13}C$-NMR, ESI-MS, and ATR-FTIR analysis, and [**Eu.L1/L2**] complexes were characterized by ESI-MS and other spectroscopic techniques (Figures S2–S19).

2.3. Photophysical Properties

The photophysical experiments of the Eu(III) probes were carried out in 10 mM HEPES buffer (pH 7.15) (Table 1). The UV-vis spectra of [**Eu.L1**] and [**Eu.L2**] showed ligand-centered transition at λ_{max} = 269 nm attributed to $\pi/n \rightarrow \pi^*$ transitions in the pyridine ring(s) aligned closely with the spectral profiles of H_2**L1**/H_2**L2** (Figure S23). This suggests nonperturbation of the deeply shielded *4f* orbitals of Eu(III) in any possible orbital overlap via chemical bonding with ligands. Instead, the ionic bonding predominantly prevails between the Eu(III) and anionic L^{2-} without any ligand-field effect. The [**Eu.L1**] and [**Eu.L2**] probes display characteristic TRL spectra due to $^5D_0 \rightarrow {}^7F_J$ (J = 0–4) transitions of Eu(III) in HEPES buffer in the red region upon excitation of the antennae at 269 and 272 nm, respectively (Figure 3b). The hypersensitive $^5D_0 \rightarrow {}^7F_2$ ED/QD transition, strongly influenced by the local symmetry and coordination environment around Eu(III), is utilized as a spectroscopic reporter for gaining insight into

Table 1. Photophysical data of [**Eu.L1**] and [**Eu.L2**] measured in 10 mM HEPES buffer (pH 7.15) at 298 K.

Complex	λ_{max}/nm	ε/$M^{-1}cm^{-1}$	$^{\tau}H_2O$[a]/ms	$^{\tau}D_2O$[a]/ms	q[b]	Φ_{em}[c]/%
[**Eu.L1**]	269	935	0.38	1.81	1.96	1.51
[**Eu.L2**]	269	4890	0.77	2.07	0.55	2.20

[a] Luminescence lifetimes at 615 nm were measured in H_2O and D_2O
[b] Values of hydration state (q) (±10%) were calculated from Horrocks' equation.[57]
[c] Quantum yields (Φ_{em}) were calculated using $Cs_3[Eu(DPA)_3]$ as a standard (Φ_{em} = 13.5 ± 1.5%),[56] errors in Φ_{em} 0.5%.

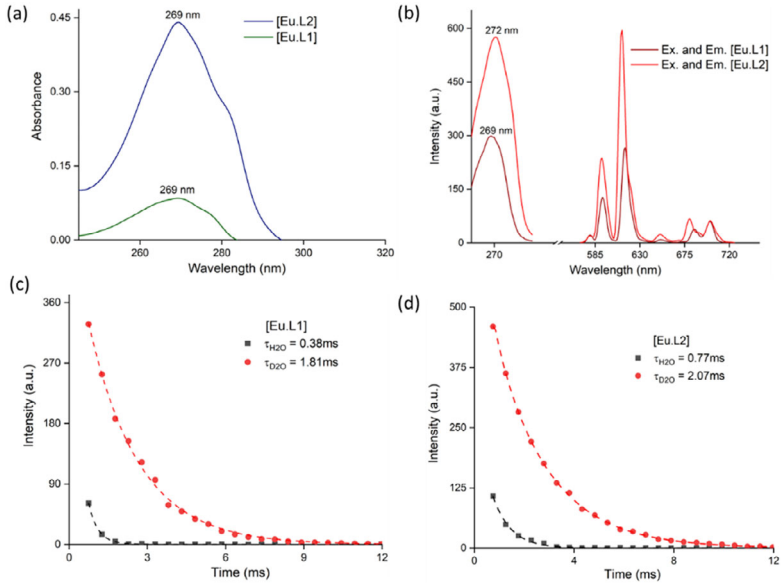

Figure 3. a) UV-Vis absorption spectra of [**Eu.L1**] (*green*) and [**Eu.L2**] (*blue*). Experimental condition: [**Eu.L**]: 0.09 M in 10 mM HEPES (pH 7.15) at 298 K. b) Excitation and time-resolved luminescence (TRL) spectra of [**Eu.L1**] (*pink*) and [**Eu.L2**] (*red*). For [**Eu.L1**], λ_{ex} = 269 nm, and for [**Eu.L2**], λ_{ex} = 272 nm, the Eu-centered emission originates from the $^5D_0 \rightarrow {}^7F_J$ (J = 0, 1, 2, 3, 4) electronic transitions are shown. c) Luminescence lifetime decay at 615 nm ($^5D_0 \rightarrow {}^7F_2$) of [**Eu.L1**] in H_2O (*black*) and in D_2O (*red*). d) Luminescence lifetime decay at 615 nm ($^5D_0 \rightarrow {}^7F_2$) of [**Eu.L2**] in H_2O (*black*) and in D_2O (*red*). Experimental condition: [**Eu.L**]: 5 μM in 10 mM HEPES buffer (pH 7.15), ex. and em. slit width = 5 nm, delay and gate time = 0.5 ms, 298 K.

the binding interaction of PPs with Eu(III) probes. The longer excited-state lifetimes of [**Eu.L1**] (τ = 0.38 ms) and [**Eu.L2**] (τ = 0.77 ms) in HEPES buffer facilitate time-gated detection of PPs with a higher S/N ratio even in the presence of relevant competitive and interfering anions (Figure 3c,d). The TRL emission intensities of [**Eu.L1**] in water at varied pH (pH 4–10) revealed $\Delta J = 2/\Delta J = 1$ remains unaffected, indicating higher structural integrity of the probes suitable for studying various PPs in biological media (Figure S25). The emission quantum yield (Φ) values of [**Eu.L1**] and [**Eu.L2**] observed ~1.51 ± 0.5% and 2.20 ± 0.5%, respectively, versus $Cs_3[Eu(DPA)_3]$ (Φ = 13.5%± 1.5%) (Table 1).[56] To examine the photostability of both the probes [**Eu.L1** and **Eu.L2**], we have monitored the TRL responses of [**Eu.L1**] and [**Eu.L2**] with a prolonged excitation at 269 nm and 272 nm. The complexes remain photostable for up to 2 hours without any apparent changes in the TRL intensity (Figures S29a, c). We also measured their photostability under continuous exposure to 354 nm UV light using TRL intensity at 615 nm without any apparent changes (Figures S29b, d), therefore confirming their significant photostability and possible photobleaching resistance under the experimental conditions used for sensing studies.

2.4. Luminescence Response of Eu(III) Probes With Inorganic Phosphates (Pi/PPi)

To assess the potentiality of Eu(III) probes for anion binding capabilities, we performed the time-resolved luminescence (TRL) titration with different biologically relevant anions in 10 mM HEPES (pH 7.15). The addition of 10 equiv. (0.05 mM) $P_2O_7^{4-}$ to [**Eu.L1**], resulting in a 60% increase in TRL intensity of the hypersensitive $^5D_0 \rightarrow {}^7F_2$ ($\Delta J = 2$) band centered at 615 nm (Figure 4c). The enhanced Eu(III) emission corresponds to the displacement of two H_2O from the Eu(III) by $P_2O_7^{4-}$, thereby preventing non-radiative VET. Whereas, upon addition of 10 equiv. (0.05 mM) of HPO_4^{2-}, no apparent changes in emission of the hypersensitive band ($\Delta J = 2$) of [**Eu.L1**] observed, indicating that the primary coordination environment around Eu(III) remains unaltered, and absence of any direct coordination via displacing H_2O molecules upon interaction with HPO_4^{2-} (Figure 4a). The direct interaction of PPs with Eu(III) via displacement of bound H_2O at first coordination sphere was directly evaluated from the changes in hydration number (q) of [**Eu.L1**] from their lifetimes (τ_{H2O} and τ_{D2O}) upon addition of various PPs using modified Horrocks' equation[57] (Table S1). The addition of $P_2O_7^{4-}$, results in

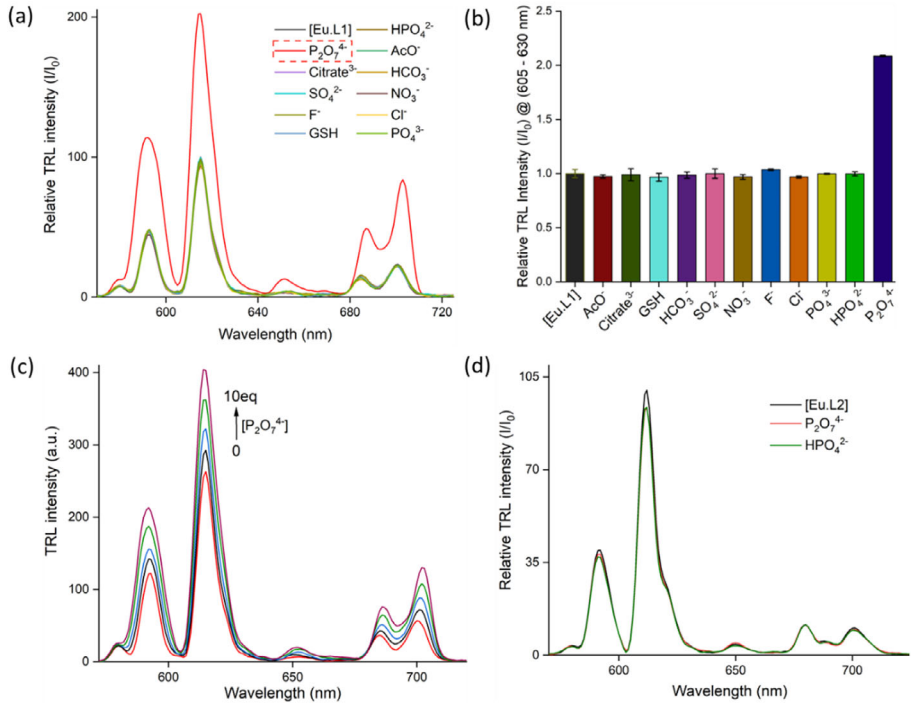

Figure 4. a), b) Selective and relative emission enhancement of [**Eu.L1**] on adding $P_2O_7^{4-}$ in the presence of common interfering anions. c) Variation of TRL intensity spectra of [**Eu.L1**] with the gradual addition of $P_2O_7^{4-}$. d) Change of TRL intensity spectra of [**Eu.L2**] with the addition of phosphates (HPO_4^{2-} & $P_2O_7^{4-}$) (0.050 mM). Conditions: [**Eu.L**]: 5 μMin 10 mM HEPES buffer (pH 7.15), λ_{ex} [**Eu.L1**] = 269 nm, λ_{ex} [**Eu.L2**] = 272 nm, ex./ em. slit width = 5 nm, delay and gate time = 0.5 ms, T = 298 K.

changes in observed q from 2 → 0 $|\Delta q = 2|$, clearly revealing the displacement of two H_2O from the first coordination sphere of [**Eu.L1**]. To gain insight on the binding interaction between [**Eu.L1**] and $[P_2O_7]^{4-}$, we measured the ^{31}P NMR spectra of the diamagnetic structural analogue [**La.L1**] in the presence of $[H_2P_2O_7]^{2-}$, showed a significant downfield shift of both the ^{31}P-nuclei, indicating possible direct coordination through the O-atoms of the $[H_2P_2O_7]^{2-}$ to the Ln(III) center (Figure 6). Based on the ^{31}P NMR experiment and changes in q values measured from lifetime experiments, we believe that the probe [**Eu.L1**] forms a 1:1 adduct with $[H_2P_2O_7]^{2-}$. The interference studies in the presence of 10 equiv. of common anions (e.g., citrate^{3-}, AcO^-, HCO_3^-, F^-, Cl^-) and biologically relevant metal ions (Mg^{2+}, Ca^{2+}, Zn^{2+}), revealed that the emission of [**Eu.L1**] remained mostly unchanged, indicating their negligible interactions (Figures 4a, b and Figure S27). Whereas, to this mixed solution of [**Eu.L1**] and common anions, the addition of 10 equiv. (0.05 mM) of $[P_2O_7]^{4-}$, the emission intensity increases by 2.1-fold, confirming its selectivity toward PPi (Figures 4a, b). While coordinatively saturated (C.N. 9) [**Eu.L2**] probe displayed only minor changes in the emission upon adding $HPO_4^-/P_2O_7^{4-}$, excluding the possibility of any direct coordination with the probe in the absence of any exchangeable inner-sphere H_2O (q < 1) (Figure 4d, Table S2).

2.5. Luminescence Response of Eu(III) Probes With Nucleoside Polyphosphates (NPPs)

To investigate how the structural variations in [**Eu.L1**] and [**Eu.L2**] affect the binding modalities, affinity, and the ability to modulate and NPP-specific ET-mechanisms (i.e., VET/PeT), we assess their ability to selectively discriminate among adenine/guanine NPPs. The continuous addition of NMPs (AMP/GMP, 0 → 0.05 mM) to [**Eu.L1**] resulted in a 40% decrease in TRL-intensity of ΔJ = 2 band. Interestingly, the addition of NDPs (ADP/ GDP, 0 → 0.05 mM) results in a 50% increase in the TRL intensity, while only minor changes were observed with NTPs (ATP/ GTP, 0–0.05 mM) (Figure 5). The q < 0.5 upon binding with NPPs suggests that the phosphate groups of NDP and NTP can displace the H_2O and directly coordinate with [**Eu.L1**], whereas NMP cannot (q ~2) (Table S1). This suggests the absence of direct binding of [**Eu.L1**] and the phosphate group of NMPs, but they remain in the vicinity of the Eu(III) probe to facilitate the PeT quenching via noncovalent π-π stacking interaction between the pyridine chromophore and purine (A/G) bases, resulting in quenching of [**Eu.L1**] luminescence intensity.[58] A minor shift of the phosphate peak in the ^{31}P NMR of GMP with [**La.L1**] probe reflects the absence of any direct bond with La(III), as perceived for Eu(III) (Figure S21). Such quenching of emission intensity by PeT via π-π interaction between the chromophoric antenna in Tb(III) probe and nucleobases in NPPs was previously reported by Pierre *et al.*[59,60] and us.[48] To gain insights into the electronic energy levels of the orbitals involved in PeT, the TRL and steady-state emission titration of A/G nucleobases with [**Eu.L1**] and **H_2L1** were studied, respectively (Figure S24, S30).

The TRL intensity of [**Eu.L1**] and the steady-state emission of **H_2L1** chelating antenna decreased with increased concentration of A/G nucleobases. This observation confirmed the presence of noncovalent π-π stacking interaction between the A/G nucleobases and the planar pyridine moiety of the **[Eu.L1]** probe and

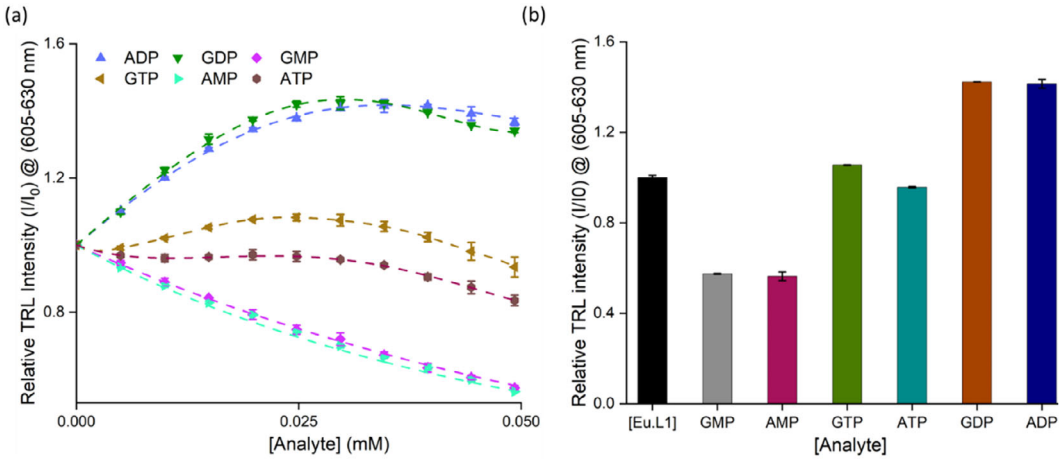

Figure 5. a) Relative changes in total TRL emission intensity (I/I_0) of [**Eu.L1**] at $\Delta J = 2$ (605 – 630 nm) versus conc. of various PPs ($C = 0$ – 0.05 mM). b) Bar diagram showcasing the relative changes in the TRL intensity (I/I_0) of [**Eu.L1**] for $^5D_0 \rightarrow {}^7F_2$ transition at $\Delta J = 2$ (605-630 nm) (*black color*) with the addition of different PPs (0.050 mM). Experimental condition [**Eu.L1**]: 5 μM in 10 mM HEPES buffer (pH 7.15), λ_{ex} [**Eu.L1**] = 269 nm, ex./ em. slit width = 5 nm, delay and gate time = 0.5 ms, $T = 298$ K.

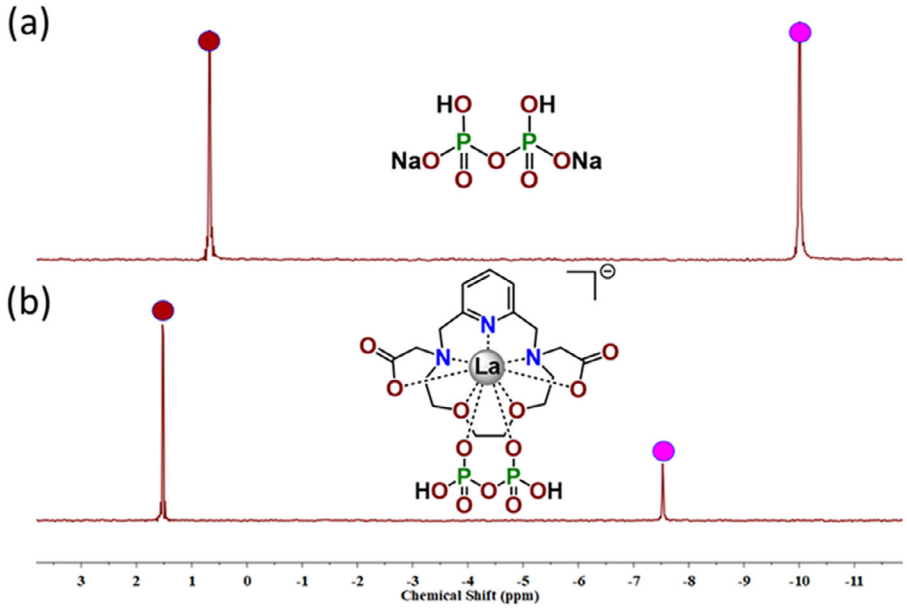

Figure 6. ^{31}P NMR of $P_2O_7^{4-}$ before a) and after b) addition of [**La.L1**] in D_2O. Downfield shift of both the phosphorous atom peaks is observed due to direct interaction of oxygens of $P_2O_7^{4-}$ at the vacant coordination sites of [**La.L1**].

H_2L1. The literature reports suggest that optimal ΔE between HOMO of A/G and the pyridine moiety is apt for effective PeT.[61,62]

The quenching of **H_2L1** antenna's emission further supports the PeT from the pyridine to purine bases (A/G) and prevents ET to Eu(III)*. Interestingly, the increase in TRL-intensity of [**Eu.L1**] with NDPs suggests that NDPs can displace the bound H_2O from the Eu(III), preventing nonradiative VET from Eu(III)* as a major modulator of the ET pathway, resulting in a *turn-ON* response. The addition of NTPs (ATP and GTP) to [**Eu.L1**] results in only ~10% increase in TRL intensity. We believe that both VET and PeT mechanisms are operative here. While the quenching of nonradiative VET of H_2O, results in enhanced TRL intensity. However, the greater flexibility of a longer phosphate chain allows NTPs to maintain the coplanarity between the nucleobases and pyridine for a favorable π-π stacking interaction and simultaneously promote the PeT quenching. These two opposite counteractive effects for ET result in only a minimal increase in the TRL intensity of [**Eu.L1**]. Thus, a coordinatively unsaturated [**Eu.L1**] probe can selectively differentiate among NMP, NDP, and NTP due to varying extents of triggered PeT and/or VET processes, thereby altering the overall luminescence response. Furthermore, we performed any discrimination between nucleoside phosphates with [**Eu.L1**] for their successive addition. The probe [**Eu.L1**] exhibits clear sequential discrimination for the successive addition of ADP, AMP, and ADP, ATP, and vice versa (Figures S26 (c-h)). However, the successive addition of GDP in the presence of ADP to [**Eu.L1**] produced invariably no changes in the hypersensitive

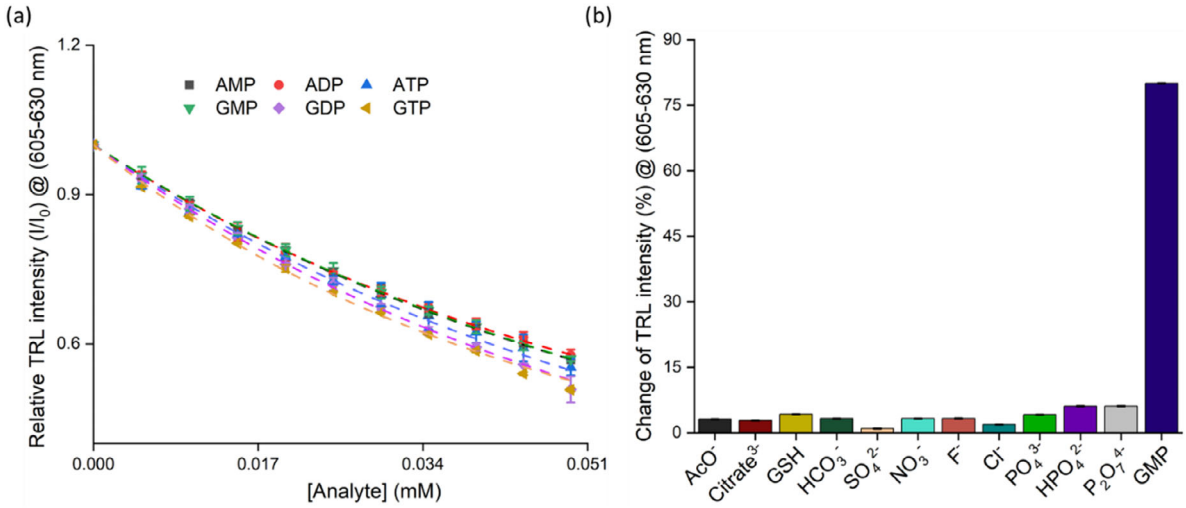

Figure 7. a) Relative changes in total TRL intensity (I/I_0) for $\Delta J = 2$ of [**Eu.L2**] versus conc. of various PPs (C = 0 – 0.05 mM). b) Selective response of [**Eu.L2**] toward GMP in the presence of interfering anions. Experimental condition: [**Eu.L2**]: 5 μM in 10 mM HEPES buffer (pH 7.15), λ_{ex} = 272 nm, slit width = 5 nm, delay and gate time = 0.5 ms, 298 K.

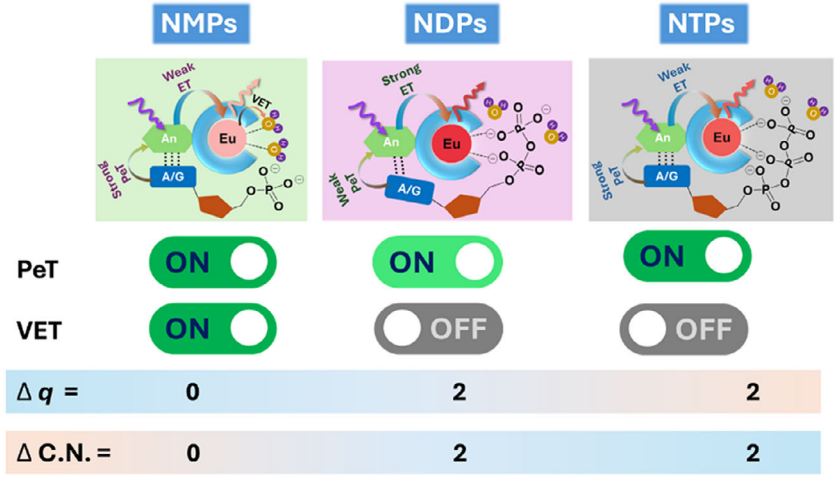

Figure 8. Proposed interaction between various NPPs with [**Eu.L1**] and responses to the respective underlying TRL modulation mechanism(s). The π-π stacking between the planar pyridine moiety and the A/G base triggered the PeT, resulting in ineffective ET to Eu(III) and luminescence quenching. The displacement of bound H_2O (q) by NPPs enhanced the TRL via quenching of the nonradiative VET pathway.

band of Eu(III) (Figure S26a, b). The successive addition of ADP and GDP does not produce any further discrimination, as both the nucleotides primarily modulate emission through the same VET-suppression mechanism. These results confirm that [**Eu.L1**] can selectively distinguish nucleotides when multiple distinct ET pathways are operative, revealing its potential for dynamic sensing of nucleotide phosphates and substrate interconversion relevant to enzymatic reactions.

In contrast, we observed only PeT-based quenching from coordinatively saturated [**Eu.L2**] (C.N. 9) in the presence of all NPPs (0–0.05 mM), with minimal possibility to expand the C.N. of Eu(III) (Figure 7a). Thus, the [**Eu.L2**] probe fails to discriminate between the NPPs, considering the comparable extent of modulation of ET via PeT pathways. The similar lifetimes (τ) and Δq ~0 were observed pre- and post-addition of NPPs, conforming with the absence of direct bonding between NPPs with Eu(III) in [**Eu.L2**] (Table S2). The ^{31}P NMR of GMP and ADP with the diamagnetic [**La.L2**] probe also negates any direct bonding between the probe and phosphates (Figures S20, S22). We presume that the NPPs present in the vicinity of the probe via π-π stacking interaction between the planar pyridine moiety with A/G bases, thereby facilitating the PeT, and quenching of luminescence via $^5D_0 \rightarrow {}^7F_J$ transitions. The steady-state emission quenching studies of **H_2L2** with NPPs also support the involvement of this PeT process (Figure S31). The time-dependent luminescence response studies of the probes with representative analytes (ADP and GMP) were conducted to evaluate their optical response kinetics and equilibration times (Figure S28). The emission profile intensity at 615 nm (ΔJ = 2 transition) reaches a stable plateau within seconds and remains unaltered thereafter. These results demonstrate that both probes display fast, diffusion-controlled binding with phosphate analytes, making them suitable for real-time rapid sensing applications.

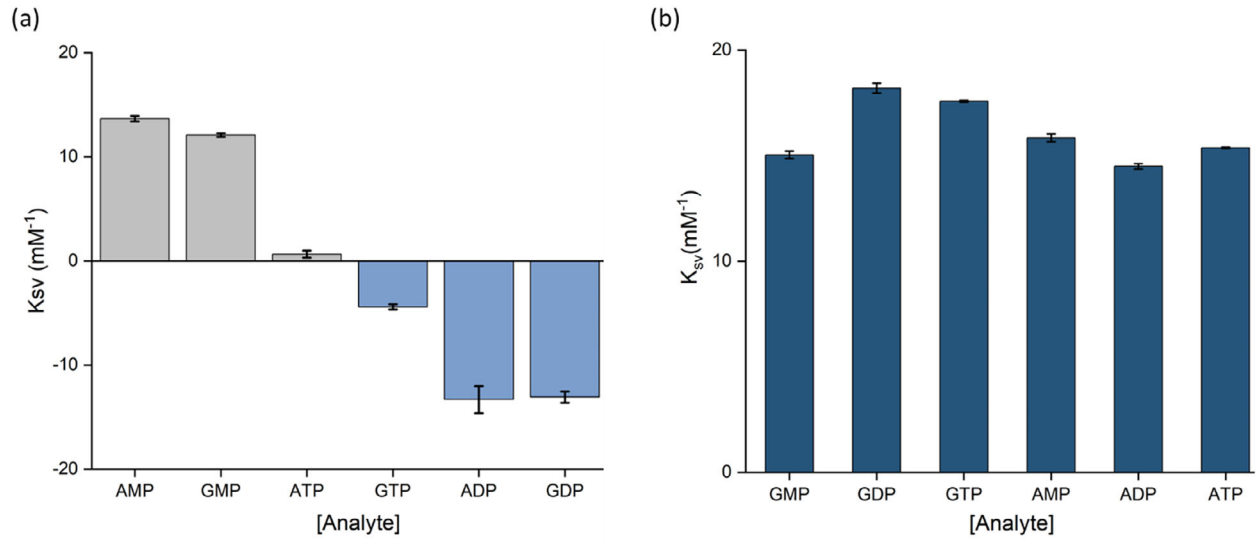

Figure 9. The Stern-Volmer quenching constant (*K*sv in mM^{-1}) a) [**Eu.L1**] with six different nucleoside phosphates; GMP and AMP show higher *K*sv values than other NPPs. b) The Stern-Volmer quenching constant (K_{SV} in mM^{-1}) of [**Eu.L2**] with six different nucleoside phosphates with comparable K_{SV} values. Experimental condition [**Eu.L**]: 5 μM in 10 mM HEPES buffer (pH 7.15), λ_{ex} [**Eu.L1**] = 269 nm, λ_{ex} [**Eu.L2**] = 272 nm, ex./ em. slit width = 5 nm, delay and gate time = 0.5 ms, T = 298 K.

The Stern-Volmer quenching constants (K_{sv}) of all the nucleotides were determined from their TRL titration data with [**Eu.L1**] and [**Eu.L2**] (Figure 9, S32). The higher K_{sv} values were observed for NMP (12.09–13.67 mM^{-1}) compared to NDP and NTP for [**Eu.L1**]. The positive and relatively higher K_{sv} values for NMPs suggest no direct coordination between the Eu(III) of [**Eu.L1**] and phosphates of NMPs, but rather binding through a weaker noncovalent π-π stacking interaction between the fluorophore pyridine and quencher adenine and guanine moieties.[60] The comparable K_{SV} values (15–18 mM^{-1}) for various NPPs with the coordinatively saturated [**Eu.L2**] probe also suggest that PeT-based quenching is operative via a noncovalent π-π stacking interaction. Figure 8 depicts the proposed binding interaction(s) of NPPs with the **[Eu.L1]** probe linked to the respective ET-pathways. The [**Eu.L1**] probe demonstrates high sensitivity toward various PPs, with limits of detection (LOD) in the nM to low μM range, with well-defined linear working ranges (~2 to 15 μM), desirable for low levels of various PPs in biological media (Figure S33, Table S3).

3. Conclusion

In conclusion, we rationally designed two water-soluble, structurally related, stable luminescent Eu(III) probes with a macrocyclic chelate appended to pyridine(s) as a chelating antenna to probe how varying binding interactions of PPs may trigger certain ET pathways and be able to discriminate various PPs. The coordinately unsaturated **[Eu.L1]** probe can selectively detect PPi ($P_2O_7^{4-}$) over Pi (HPO_4^{2-}) via arresting nonradiative VET from Eu(III)* to H_2O. **[Eu.L1]** can also differentiate within NPPs (NMPs, NDPs, NTPs) via the cumulative effect of VET and/or PeT pathways. The coordinatively saturated [**Eu.L2**] selectively differentiates between Pi and NPPs through TRL-quenching of Eu(III) probe via an exclusive PeT process. The study reinforces the importance of subtle design criteria of bioresponsive luminescent Ln(III) probes, targeted to specific modulation of ET-pathways for affecting discrimination and real-time monitoring of critical PPs in biology. The exploitation and targeting of analyte-specific EnT-mechanism(s) or their combination linked to their differential molecular interaction(s) with an emissive Ln(III) probe is a unique TRL-probe design strategy to achieve challenging discrimination among structurally analogous Pi or NPPs in a physiological milieu for biomedical research. Overall, this work presents a rational design approach for uniquely advantageous luminescent lanthanide probes for the detection, discrimination, and real-time monitoring of challenging and structurally analogous nucleotides in physiological media, underscoring their utility in studying a plethora of biochemical processes, drug discovery, and diagnosis.

4. Experimental section

General methods: All the high-purity grade reagents and HPLC/spectroscopic grade solvents are procured from commercial suppliers and utilized without additional purification. Anhydrous solvents are prepared using conventional established procedures. Inorganic phosphates, viz. di-sodium hydrogen orthophosphate dihydrate ($Na_2HPO_4.2H_2O$) (Pi) and di-sodium dihydrogen pyrophosphate ($Na_2H_2P_2O_7$) (PPi), are purchased from Avra and Finar chemicals. Nucleoside phosphates like adenosine triphosphate disodium salt (ATP), adenosine diphosphate sodium salt (ADP), adenosine monophosphate hydrate (AMP), guanosine triphosphate disodium salt dihydrate (GTP), guanosine diphosphate disodium salt (GDP), and guanosine monophosphate disodium salt (GMP) are acquired from Sigma-Aldrich (Merck). The silica gel (100- 200 mesh) used in column chromatography was purchased from Finar Chemicals. TLC plates with F254 fluorescent indicators are procured from Merck. The HEPES buffer (10 mM, pH 7.15) was prepared

using distilled water. ChemDraw v21.0.0.28, OriginPro 2021 (64 bit) v9.8.0.200, and MestreNova v6.0.2–5475, software were used to create plots and graphical representations.

Synthesis of Macrocylic Chelates (H_2L1 and H_2L2) and Eu(III) Probes (Eu.L1 and Eu.L2): The overall stepwise synthetic scheme and compound labels were given in Figure 2. The intermediates **1–3** were prepared from previously reported literature and characterized as described in the SI and used in the successive steps described in detail here.[50–54].

Synthesis of **4**: The compound **4** was synthesized using a modified literature procedure.[55] In a 250 mL R.B., 2,2′-(ethane-1,2-diylbis(oxy))bis(ethan-1-amine) (4 mL, 26.99 mmol) was dissolved in 50 mL of dry DCM, and triethylamine (9.48 mL) was added, and the flask was cooled to 0 °C in an ice bath. 2-nitrobezenesufonyl chloride (*o*-NsCl) (11.96 g, 53.98 mmol) was dissolved in 50 mL of dry DCM and added dropwise through a dropping funnel for 1 hour. During the addition, the colorless solution turns yellow, and the reaction mixture is allowed to stir overnight at RT. Thereafter, the reaction mixture was extracted using a DCM/water system. The organic layer was dried over anh. Na_2SO_4 and evaporated with a rotary evaporator to yield compound **4** as a crude yellow oil. The crude mixture was purified using silica gel column chromatography with a 60% ethyl acetate/hexane mixture, which afforded compound **4** as a white crystalline solid (13 g, yield: 92%). ^{1}H NMR (400 MHz, $CDCl_3$) δ 8.13 – 8.11 (m, 2H), 7.88 – 7.86 (m, 2H), 7.74 – 7.72 (m, 4H), 5.90 (s, 2H), 3.56 (t, J = 5.0 Hz, 4H), 3.50 (s, 4H), 3.26 (dd, J = 10.1, 5.2 Hz, 4H). ^{13}C NMR (101 MHz, $CDCl_3$) δ 148.07, 133.76, 133.61, 132.97, 131.12, 125.62, 70.43, 69.28, 43.60 (Figure S7).

Synthesis of **5**: In a 50 mL R.B., compound **4** (1 g, 1.93 mmol) was dissolved in 25 mL dry acetonitrile and anhy. K_2CO_3 (1.07 g, 7.71 mmol) was added and stirred for 30 minutes at RT under an inert atmosphere. After 30 minutes, 2,6-bis(bromomethyl)pyridine (**3a**) (511 mg, 1.93 mmol) was dissolved in 5 mL dry acetonitrile and added dropwise to the reaction mixture through a syringe. Then, the reaction mixture was refluxed overnight under N_2 atmosphere. Thereafter, the reaction mixture was filtered to remove the excess salt, and the solvent was evaporated to yield a yellow-colored oily product. The crude mixture was extracted with DCM/water, and the organic phase was dried over anh. Na_2SO_4. The evaporation of the solvent with a rotary evaporator afforded compound **5** as a yellow-colored oily crude product. The crude mixture was purified using silica gel column chromatography (80% ethyl acetate/hexane mixture) to yield compound **5** as a white powder (1.10 g, yield: 91%). ^{1}H NMR (400 MHz, $CDCl_3$) δ 8.07 – 7.96 (m, 2H), 7.74 – 7.51 (m, 7H), 7.41 (d, J = 7.8 Hz, 2H), 4.63 (d, J = 5.9 Hz, 4H), 3.59 – 3.53 (m, 4H), 3.48 – 3.44 (m, 4H), 3.22 (d, J = 31.4 Hz, 4H). ^{13}C NMR (101 MHz, $CDCl_3$) δ 156.36, 148.41, 137.66, 133.81, 133.06, 131.91, 131.02, 124.46, 121.30, 70.51, 70.40, 55.60, 49.49 (Figure S8).

Synthesis of **6**: Compound **6** was synthesized using literature procedure.[55] In a 50 mL R.B., compound 5 (2 g, 3.22 mmol) was dissolved in 30 mL dry acetonitrile, anhy. K_2CO_3 (1.78 g, 12.87 mmol). Thiophenol (0.82 mL, 8.04 mmol) was added subsequently under an N_2 atm, resulting in a colorless solution that turned yellow. The reaction was stirred overnight at RT. Thereafter, the reaction mixture was filtered to remove the precipitate, and the solvent was evaporated to yield a yellow-colored gummy solid. The reaction mixture was dissolved in water and acidified with 1 N HCl solution, kept at pH 3, and extracted with ethyl acetate until the solution was transparent. The solution was then basified with 2 N NaOH, kept at pH 10, and extracted again with DCM. The organic layer was dried over anhy. Na_2SO_4 and concentrated in a rotatory evaporator to give compound **6** as an oily crude product. The purification was done with silica gel column chromatography in a 10% methanol/DCM mixture as an eluent to give compound **6** as a colorless oily product (600 mg, yield: 74%). ^{1}H NMR (400 MHz, $CDCl_3$) δ 7.53 (t, J = 7.6 Hz, 1H), 7.01 (d, J = 7.7 Hz, 2H), 3.90 (s, 4H), 3.70 – 3.68 (m, 4H), 3.64 (s, 4H), 2.85 – 2.83 (m, 4H). ^{13}C NMR (101 MHz, $CDCl_3$) δ 157.79, 136.74, 120.28, 70.31, 70.10, 53.69, 49.22 (Figure S9).

Synthesis of **7a**: Compound **7a** was synthesized using the literature procedure with some modifications.[49] In a 50 mL R.B., compound **6** (500 mg, 1.99 mmol) and anhy. K_2CO_3 (1.10 g, 7.96 mmol) was dissolved in 25 mL dry acetonitrile and stirred at room temperature for 0.5 hours under N_2 atm. After 0.5 hours, methyl bromoacetate (0.39 mL, 4.18 mmol) was added dropwise and stirred at 60 °C overnight. After that, filtration was performed to remove the excess salt, and evaporation of the solvent gave a yellow gummy solid. The crude mixture was extracted with DCM/water, and the organic phase was dried over anh. Na_2SO_4. The solvent was evaporated in a rotavac and afforded compound **7a** as a brown-colored oily crude product. The crude mixture was purified using silica gel column chromatography (5% methanol/DCM mixture) to give compound 7a as a colorless oil (690 mg, yield: 87%). ^{1}H NMR (400 MHz, $CDCl_3$) δ 7.63 (t, J = 7.6 Hz, 1H), 7.12 (d, J = 7.7 Hz, 2H), 3.97 – 3.46 (m, 22H), 2.94 – 2.82 (m, 4H). ^{13}C NMR (101 MHz, $CDCl_3$) δ 173.21, 157.88, 138.12, 122.20, 69.32, 66.85, 58.83, 56.59, 54.44, 52.68 (Figure S10).

Synthesis of **7b**: In a 50 mL R.B., compound **6** (500 mg, 1.99 mmol) was dissolved in 25 mL dry acetonitrile and anh. K_2CO_3 (1.10 g, 7.96 mmol) was added and stirred for 30 minutes at RT under an inert atmosphere. After 30 minutes, methyl 6-(bromomethyl) picolinate (**3b**) (962 mg, 4.18 mmol) was dissolved in 10 mL dry acetonitrile and added dropwise to the reaction mixture through a syringe. Then, the reaction mixture was refluxed overnight under N_2 atm. Thereafter, the reaction mixture was filtered to remove the excess salt, and the solvent was evaporated to yield a brown-colored oil. The crude mixture was extracted with DCM/water, and the organic phase was dried over anh. Na_2SO_4. The evaporation of solvent afforded compound **7b** as a brown-colored, oily crude product. The crude mixture was purified using silica gel column chromatography (10% methanol/DCM mixture) to yield compound **7b** as a yellow-colored oily product (750 mg, yield: 78%). ^{1}H NMR (400 MHz, $CDCl_3$) δ 7.84 (d, J = 7.7 Hz, 2H), 7.72 (t, J = 7.7 Hz, 2H), 7.63 (t, J = 7.7 Hz, 1H), 7.50 (d, J = 7.7 Hz, 2H), 7.13 (d, J = 7.7 Hz, 2H), 4.01 (d, J = 27.0 Hz, 8H), 3.76 (s, 6H), 3.63 (d, J = 29.9 Hz, 8H), 2.81 (t, J = 4.7 Hz, 4H). ^{13}C NMR (101 MHz, $CDCl_3$) δ 165.59, 158.58, 158.32, 146.90, 138.27, 138.00, 127.03, 123.76, 122.15, 69.18, 67.09, 59.73, 58.84, 54.09, 52.94, 29.73 (Figure S11).

Synthesis of **H_2L1**: Ligand **H_2L1** was synthesized according to the literature procedure.[52] In a 25 mL R.B., compound **7a** (500 mg, 1.26 mmol) was dissolved in 10 mL 6 M HCl and heated at 100 °C for 72 hours. Thereafter, the solvent was removed with a rotary evaporator, and diethyl ether was added to solidify the compound with trituration. The ligand **H_2L1** was extracted as a white hygroscopic product and stored in a desiccator (530 mg, yield: 95%). ^{1}H NMR (400 MHz, D_2O) δ 7.95 (t, J = 7.9 Hz, 1H), 7.48 (d, J = 7.8 Hz, 2H), 4.21 (s, 4H), 3.88 – 3.69 (dd, J = 39.1, 34.3 Hz, 16H). ^{13}C NMR (101 MHz, D_2O) δ 168.38, 149.03, 140.36, 124.20, 69.45, 62.97, 57.03, 55.39, 54.74 (Figure S12). ATR-FTIR (cm^{-1}): 3350 ($\nu_{O\text{-}H}$), 3100 ($\nu_{Csp2\text{-}H}$), 2950 ($\nu_{Csp3\text{-}H}$),1640 ($\nu_{C=O}$), 1100 ($\nu_{C\text{-}O}$) (Figure S18 (a)). ESI-MS (+) in H_2O: *m/z* $[M + Na]^+$ exp.: 390.1643, calcd.: 390.1636 (Figure S14). UV-vis (10 mM HEPES, pH 7.15): λ_{max} (ε/Lmol^{-1}cm^{-1}) = 264 nm (3263), 269 (2895) (Figure S23).

Synthesis of **H_2L2**: Ligand **H_2L2** was synthesized from 7b (500 mg, 0.90 mmol) using the same procedure as **H_2L1** (530 mg, yield: 98%). ^{1}H NMR (400 MHz, D_2O) δ 7.55 (d, J = 7.7 Hz, 2H), 7.35 (t, J = 7.7 Hz, 1H), 7.27 (t, J = 6.9 Hz, 2H), 7.14 (d, J = 7.7 Hz, 2H), 6.80 (d, J = 7.7 Hz, 2H), 3.65 (d, J = 66.4 Hz, 16H), 2.69 (s, 4H). ^{13}C NMR (101 MHz, D_2O) δ 169.29, 152.30, 152.16, 149.17, 142.41, 142.22, 128.30, 126.66, 71.96, 65.67, 59.81, 58.04 (Figure S13). ATR-FTIR (cm^{-1}):

3342 ($\nu_{O\text{-}H}$), 3100 ($\nu_{Csp2\text{-}H}$), 2924 ($\nu_{Csp3\text{-}H}$),1732 ($\nu_{C=O}$), 1614 ($\nu_{C=N}$), 1100 ($\nu_{C\text{-}O}$) (Figure S18 (b)). ESI-MS (+) in H_2O: *m/z* $[M + H]^+$ exp.: 522.2347, calcd.: 522.2348 (Figure S15). UV-vis (10 mM HEPES, pH 7.15): λ_{max} (ε/Lmol^{-1}cm^{-1}) = 267 nm (7105) (Figure S23).

Synthesis of [**Eu.L1**]: In a 25 mL R.B., ligand **H_2L1** (36.74 mg, 0.1 mmol) was dissolved in 5 mL of water, and the pH of the solution was adjusted to 7 using a $NaHCO_3$ solution. $EuCl_3{\cdot}6H_2O$ (36.64 mg, 0.1 mmol) was dissolved in 2 mL of water and added dropwise to the ligand solution. The reaction was stirred overnight at 50 °C. Then, the mixture was filtered to remove any precipitate formed, and the filtrate was concentrated under vacuum, yielding the [**Eu.L1**] complex as a white hygroscopic product (50 mg, yield: 90%). The complex was characterized by ESI-MS and ATR-FTIR techniques. ATR-FTIR (cm^{-1}): 3240 ($\nu_{O\text{-}H}$), 2960 ($\nu_{Csp3\text{-}H}$), 1575 ($\nu_{C=O}$), 1055 ($\nu_{C\text{-}O}$) (Figure S19 (a)). ESI-MS (+)ve in H_2O: *m/z* $[M]^+$ exp.: 518.0796, calcd.: 518.0799 (Figure S16). UV-vis (10 mM HEPES, pH 7.15): λ_{max} (ε/Lmol^{-1}cm^{-1}) = 269 nm (935) (Figure 3(a), Table 1).

Synthesis of [**Eu.L2**]: The [**Eu.L2**] complex was also prepared using a similar procedure described for [**Eu.L1**] as a light-yellow hygroscopic product. The [**Eu.L2**] complex was also characterized by ESI-MS and ATR-FTIR. ATR-FTIR (cm^{-1}): 3400 ($\nu_{O\text{-}H}$), 3080 ($\nu_{Csp2\text{-}H}$), 2890 ($\nu_{Csp3\text{-}H}$), 1630 ($\nu_{C=O}$), 1060 ($\nu_{C\text{-}O}$) (Figure S19 (b)). ESI-MS (+)ve in H_2O: *m/z* $[M]^+$ exp.: 672.1348, calcd.: 672.1330 (Figure S17). UV-vis (10 mM HEPES, pH 7.15): λ_{max} (ε/Lmol^{-1}cm^{-1}) = 269 nm (4890) (Figure 3(a), Table 1).

Supporting Information

The data supporting this article have been included as part of the SI.

Acknowledgments

The authors would like to thank the Anusandhan National Research Foundation for financial support (CRG/2021/000527). G.P. thanks PMRF for the fellowship. S.P. and N.S. acknowledge UGC and CSIR for research fellowships.

Conflict of Interest

There are no conflicts to declare.

Data Availability Statement

The data that support the findings of this study are available in the supplementary material of this article.

Keywords: Europium · Luminescence · Photo-induced electron transfer (PeT) · Physiological phosphates · Vibrational energy transfer (VET)

[1] K. G. Wagner, T. Pesnot, *ChemBioChem* **2010**, *11*, 1939. https://doi.org/10.1002/cbic.201000201.
[2] Y. Zhou, Z. Xu, J. Yoon, *Chem. Soc. Rev.* **2011**, *40*, 2222. https://doi.org/10.1039/c0cs00169d.
[3] A. M. Agafontsev, A. Ravi, T. A. Shumilova, A. S. Oshchepkov, E. A. Kataev, *Chem. Eur. J.* **2019**, *25*, 2684. https://doi.org/10.1002/chem.201802978.
[4] M. V. Ramakrishnam Raju, S. M. Harris, V. C. Pierre, *Chem. Soc. Rev.* **2020**, *49*, 1090. https://doi.org/10.1039/C9CS00543A.
[5] T. L. M. Martinon, V. C. Pierre, *Chem. – Asian J* **2022**, *17*, e202200495. https://doi.org/10.1002/asia.202200495.
[6] S. Muller, A. Chaikuad, N. S. Gray, S. Knapp, *Nat. Chem. Biol.* **2015**, *11*, 818. https://doi.org/10.1038/nchembio.1938.
[7] M. Rroji, A. Figurek, D. Viggiano, G. Capasso, G. Spasovski, *Int. J. Mol. Sci.* **2022**, *23*, 7362. https://doi.org/10.3390/ijms23137362.
[8] S. H. Hewitt, R. Ali, R. Mailhot, C. R. Antonen, C. A. Dodson, S. J. Butler, *Chem. Sci.* **2019**, *10*, 5373. https://doi.org/10.1039/C9SC01552C.
[9] R. N. Foley, *Clin. J. Am. Soc. Nephrol.* **2009**, *4*.
[10] G. A. Block, F. K. Port, *Am. J. Kidney Dis.* **2000**, *35*, 1226. https://doi.org/10.1016/S0272-6386(00)70064-3.
[11] A. Akedeniz, M. G. Caglayan, I. Polivina, P. Anzenbacher, *Org. Biomol. Chem.* **2016**, *14*, 7459. https://doi.org/10.1039/C6OB01378C.
[12] T. Sakamoto, A. Ojida, I. Hamachi, *Chem. Commun.* **2009**, 141. https://doi.org/10.1039/B812374H.
[13] A. E. Hargrove, S. Nieto, T. Zhang, J. L. Sessler, E. V. Anslyn, *Chem. Rev.* **2011**, *111*, 6603, https://doi.org/10.1021/cr100242s.
[14] S. J. Butler, D. Parkar, *Chem. Soc. Rev.* **2013**, *42*, 1652. https://doi.org/10.1039/C2CS35144G.
[15] S. M. Butler, K. A. Jolliffe, in *Fluorescent Chemosensors for Phosphates*, **2023**, pp. 198–232, Royal Society of Chemistry.
[16] M. Pushina, S. Farshbaf, W. Mochida, M. Kanakubo, R. Nishiyabu, Y. Kubo, P. Anzenbacher Jr., *Chem. Eur. J.* **2021**, *27*, 11344. https://doi.org/10.1002/chem.202100896.
[17] L. Reinke, M. Koch, C. Müller-Renno, S. Kubik, *Org. Biomol. Chem.* **2021**, *19*, 3893. https://doi.org/10.1039/D1OB00341K.
[18] M. Strianese, S. Milione, A. Maranzana, A. Grassi, C. Pellecchia, *Chem. Commun.* **2012**, *48*, 11419. https://doi.org/10.1039/c2cc35730e.
[19] X. Zhang, J. Liu, J. Wang, L. Han, S. Ma, M. Zhao, G. Xi, *J. Photochem. Photobiol. B.* **2021**, *223*, 112279 https://doi.org/10.1016/j.jphotobiol.2021.112279.
[20] J.-C. G. Bunzli, *Acc. Chem. Res.* **2006**, *39*, 53. https://doi.org/10.1021/ar0400894.
[21] E. G. Moore, A. P. S. Samuel, K. N. Raymond, *Acc. Chem. Res.* **2009**, *42*, 542. https://doi.org/10.1021/ar800211j.
[22] A. B. Aletti, D. M. Gillen, T. Gunnlaugsson, *Coord. Chem. Rev.* **2018**, *354*, 98. https://doi.org/10.1016/j.ccr.2017.06.020.
[23] D. Parkar, J. D. Fradgley, K.-L. Wong, *Chem. Soc. Rev.* **2021**, *50*, 8193. https://doi.org/10.1039/D1CS00310K.
[24] M. C. Heffern, L. M. Matosziuk, T. J. Meade, *Chem. Rev.* **2014**, *114*, 4496. https://doi.org/10.1021/cr400477t.
[25] J.-C. Bunzli, *Coord. Chem. Rev.* **2015**, *19*:293.
[26] M. H. V. Werts, *Sci. Prog. (1933-)* **2005**, *88*, 101. https://doi.org/10.3184/003685005783238435.
[27] H. Xu, Q. Sun, Z. An, Y. Wei, X. Liu, *Coord. Chem. Rev.* **2015**, *293-294*, 228. https://doi.org/10.1016/j.ccr.2015.02.018.
[28] M. L. Aulsebrook, B. Graham, M. R. Grace, K. L. Tuck, *Coord. Chem. Rev.* **2018**, *375*, 191. https://doi.org/10.1016/j.ccr.2017.11.018.
[29] U. Cho, J. K. Chen, *Cell Chem. Bio.* **2020**, *27*, 921. https://doi.org/10.1016/j.chembiol.2020.07.009.
[30] N. Shukla, V. Singhmar, J. Sayala, A. K. Patra, *Inorg. Chem.* **2025**, *64*, 1287. https://doi.org/10.1021/acs.inorgchem.4c03955.
[31] N. Shukla, J. Sayala, G. Panigrahi, A. K. Patra, *J. Mater. Chem. C* **2025**, Advance Article, https://doi.org/10.1039/D5TC02283E.
[32] U. Yadav, Z. Abbas, R. J. Butcher, A. K. Patra, *Sens. Actuators B: Chem.* **2023**, *375*, 132938. https://doi.org/10.1016/j.snb.2022.132938.
[33] K. Gupta, A. K. Patra, *ACS Sens.* **2020**, *5*, 1268. https://doi.org/10.1021/acssensors.9b02552.
[34] Z. Abbas, U. Yadav, R. J. Butcher, A. K. Patra, *J. Mater. Chem. C* **2021**, *9*, 10037. https://doi.org/10.1039/D1TC01685G.
[35] C. Alexander, Z. Guo, P. B. Glover, S. Faulkner, Z. Pikramenou, *Chem. Rev.* **2025**, *125*, 2269. https://doi.org/10.1021/acs.chemrev.4c00615.
[36] S. E. Bodman, S. J. Butler, *Chem. Sci.* **2021**, *12*, 2716.
[37] S. H. Hewitt, G. Macey, R. Mailhot, M. R. J. Eslsegood, F. Duarte, A. M. Kenwright, S. J. Butler, *Chem. Sci.* **2020**, *11*, 3619. https://doi.org/10.1039/D0SC00343C.

[38] S.-Y. Huang, M. Qian, V. C. Pierre, *Inorg. Chem.* **2020**, *59*, 4096. https://doi.org/10.1021/acs.inorgchem.0c00137.
[39] M. L. Aulsebrook, M. Starck, M. R. Grace, B. Graham, P. Thordarson, R. Pal, K. L. Tuck, *Inorg. Chem.* **2018**, *58*, 495. https://doi.org/10.1021/acs.inorgchem.8b02731.
[40] L. J. Charbonniere, R. Schurhammer, S. Mameri, G. Wipff, R. F. Ziessel, *Inorg. Chem.* **2005**, *44*, 7151. https://doi.org/10.1021/ic051033o.
[41] J. Sahoo, C. Krishnaraj, J. Sun, B. B. Panda, P. S. Subramanian, H. S. Jena, *Coord. Chem. Rev.* **2022**, *466*, 214583. https://doi.org/10.1016/j.ccr.2022.214583.
[42] S. Pal, T. K. Ghosh, R. Ghosh, S. Mondal, P. Ghosh, *Coord. Chem. Rev.* **2020**, *405*, 213128. https://doi.org/10.1016/j.ccr.2019.213128.
[43] J. Sahoo, S. Jaiswar, H. S. Jena, P. S. Subramanian, *ChemistrySelect* **2020**, *5*, 12878 https://doi.org/10.1002/slct.202002714.
[44] Y.-W. Wang, S.-B. Liu, Y.-L. Yang, P.-Z. Wang, A.-J. Zhang, Y. Peng, *ACS Appl. Mater. Interfaces* **2015**, *7*, 4415. https://doi.org/10.1021/am5089346.
[45] J. Sahoo, R. Arunachalam, P. S. Subramanian, E. Suresh, A. Valkonen, K. Rissanen, M. Albrecht, *Angew. Chem. Int. Ed.* **2016**, *55*, 9625. https://doi.org/10.1002/anie.201604093.
[46] S.-Y. Huang, M. Qian, V. C. Pierre, *Inorg. Chem.* **2019**, *58*, 16087. https://doi.org/10.1021/acs.inorgchem.9b02650.
[47] S. E. Bodman, P. Stachelek, U. Rehman, F. Plasser, R. Pal, S. J. Butler, *Chem. Sci.* **2025**, *16*, 5602. https://doi.org/10.1039/D4SC07188C.
[48] S. Pradhan, N. Shukla, G. Panigrahi, A. K. Patra, *Chem. Commun.* **2025**, *61*, 1886. https://doi.org/10.1039/D4CC05232C.
[49] P. Antal, B. Drahoš, R. Herchel, Z. Trávníček, *Eur. J. Inorg. Chem.* **2018**, 4286. https://doi.org/10.1002/ejic.201800769.
[50] Z. Kokan, M. J. Chmielewski, *J. Am. Chem. Soc.* **2018**, *140*, 16010. https://doi.org/10.1021/jacs.8b08689.
[51] H. Su, C. Wu, J. Zhu, T. Miao, D. Wang, C. Xia, X. Zhao, Q. Gong, B. Song, H. Ai, *Dalton Trans.* **2012**, *41*, 14480. https://doi.org/10.1039/c2dt31696j.
[52] N. Choudhary, H. Scheiber, J. Zhang, B. O. Patrick, M. de Guadalupe Jaraquemada-Peláez, C. Orvig, *Inorg. Chem.* **2021**, *60*, 12855. https://doi.org/10.1021/acs.inorgchem.1c01175.
[53] Y. Y. Zhu, X. D. Wu, S.-X. Gu, L. Pu, *J. Am. Chem. Soc.* **2019**, *141*, 175. https://doi.org/10.1021/jacs.8b07803.
[54] S. Dindar, A. N. Kharat, S. Zamanian, J. Janczak, *Inorg. Chem. Commun.* **2021**, *134*, 108943. https://doi.org/10.1016/j.inoche.2021.108943.
[55] J. M. Siaugue, F. Segat-Dioury, I. Sylvestre, A. Favre-Reguillon, J. Foos, C. Madic, A. Guy, *Tetrahedron* **2001**, *57*, 4713. https://doi.org/10.1016/S0040-4020(01)00328-3.
[56] A. Chauvin, F. Gumy, D. Imbert, J. G. Bunzli, *Spectrosc. Lett.* **2004**, *37*, 517. https://doi.org/10.1081/SL-120039700.
[57] W. D. Horrocks, Jr., D. R. Sudnick, *J. Am. Chem. Soc.* **1979**, *101*, 334. https://doi.org/10.1021/ja00496a010.
[58] M. Inclan, M. T. Albelda, E. Carbonell, S. Blasco, A. Bauza, A. Frontera, E. G- Espana, *Chem. Eur. J.* **2014**, *20*, 3730. https://doi.org/10.1002/chem.201303861.
[59] E. A. Weitz, J. Y. Chang, A. H. Rosenfield, V. C. Pierre, *J. Am. Chem. Soc.* **2012**, *134*, 16099. https://doi.org/10.1021/ja304373u.
[60] E. A. Weitz, J. Y. Chang, A. H. Rosenfield, E. A. Morrow, V. C. Pierre, *Chem. Sci.* **2013**, *4*, 4052. https://doi.org/10.1039/c3sc51583d.
[61] D. Chen, S.-J. Su, Y. Cao, *J. Mater. Chem. C* **2014**, *2*, 9565. https://doi.org/10.1039/C4TC01941E.
[62] A. Del Prado, D. Gonzalez - Rodriguez, Y.-L. Wu, *ChemistryOpen* **2020**, *9*, 409. https://doi.org/10.1002/open.201900363.

Manuscript received: July 31, 2025
Revised manuscript received: November 6, 2025
Version of record online: ■■, ■■